THE JOURNAL OF PHYSICAL CHEMISTRY Letters

Letter

pubs.acs.org/JPCL

The Molecular Volcano Revisited: Determination of Crack Propagation and Distribution During the Crystallization of Nanoscale Amorphous Solid Water Films

R. Alan May, R. Scott Smith,* and Bruce D. Kay*

Fundamental and Computational Sciences Directorate, Pacific Northwest National Laboratory, P.O. Box 999, Mail Stop K8-88, Richland, Washington 99352, United States

ABSTRACT: Temperature programmed desorption (TPD) is utilized to determine the length distribution of cracks formed through amorphous solid water (ASW) during crystallization. This distribution is determined by monitoring how the thickness of an ASW overlayer alters desorption of an underlayer of O_2. As deposited, ASW prevents desorption of O_2. During crystallization, cracks form through the ASW and open a path to vacuum, which allows O_2 to escape in a rapid episodic release known as the "molecular volcano". Sufficiently thick ASW overlayers further trap O_2 resulting in a second, higher temperature, O_2 desorption peak. The evolution of this trapping peak with overlayer thickness is the basis for determining the length distribution of crystallization-induced cracks spanning the ASW. Reflection absorption infrared spectroscopy (RAIRS) and TPD of multicomponent parfait structures of ASW, O_2, and Kr indicate that a preponderance of these cracks propagate down from the outer surface of the ASW.

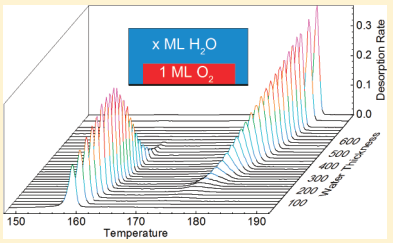

SECTION: Surfaces, Interfaces, Catalysis

Amorphous solid water (ASW) is a kinetically metastable form of water formed when H_2O impinges on a surface cooled below 130 K, and is the most abundant form of H_2O in the universe.[1−3] ASW forming on grains of dust in the interstellar medium (ISM) may play an important role in the formation and collection of molecules that are essential to an array of astrophysical processes.[4−6] For example, the trapping of O_2 by ASW may be of paramount importance to explaining the low abundance of molecular oxygen detected in the ISM and why significant quantities have been detected only in relatively warm regions of the Orion nebula.[7] When O_2 is covered by ASW, O_2 desorption is delayed until crystallization-induced cracking of the ASW releases the O_2 in a rapid episodic event termed the "molecular volcano".[8−10] Herein, temperature programmed desorption (TPD) and reflection absorption infrared spectroscopy (RAIRS) are utilized in concert to understand how the crystallization of ASW leads to the release of O_2. We demonstrate a previously unreported method for determining the length distribution of cracks spanning through the ASW and, by utilizing well-controlled molecular beam deposition of parfait structures, show that crystallization-induced cracking initiates at the ASW surface. These findings not only impact astrophysical problems, but touch on fundamental questions about ASW and crystallization.[1−3,11−15]

The large shift in desorption temperature that occurs when O_2 is covered by ASW is illustrated in Figure 1. One monolayer of O_2 deposited on graphene at 25 K has a desorption peak of 48 K at a ramp rate of 1 K/s. However, when covered by 340 ML of ASW, desorption of O_2 is delayed by the ASW overlayer until two peaks are detected at 163 and 180 K. The peak at 163 K is an example of the "molecular volcano" which occurs as the kinetically metastable ASW crystallizes into thermodynamically stable crystalline ice. This process of crystallization induces cracks through the ASW overlayer allowing O_2 to escape.[10] The second peak, 180 K, occurs concomitant with the end of H_2O desorption and is attributed to O_2 trapped beneath the H_2O that could not escape during the molecular volcano. Minimal O_2 desorption is observed between the two desorption peaks. This indicates that the majority of trapped O_2 is concentrated at

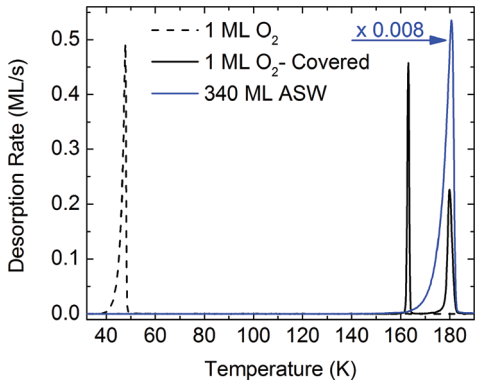

Figure 1. (a) TPD of 1 ML O_2 from graphene (dashed line) and 1 ML of O_2 covered by 340 ML ASW (black line). Also shown is the water TPD (blue line) rescaled by a factor of 0.008. The heating rates were 1 K/s. When covered, desorption of O_2 is split between the molecular volcano at ∼162 K and an amount trapped beneath ASW.

Received: December 14, 2011
Accepted: January 11, 2012
Published: January 11, 2012

the bottom of the ASW. However, for the range of thicknesses tested, desorption of trapped O_2 occurs commensurate with desorption of the last ~100 ML of ASW, indicating mixing at the O_2/ASW interface. Similar trapping and mixing behavior was observed by McClure et al. who used the trapping of CCl_4 to estimate the ASW crystallization-induced crack length and the correlation of the volcano peak with crystallization.[14] Their results, along with some of our previous work,[8] suggest that the crystallization-induced desorption mechanism is independent of the trapped gas. Below, ternary systems will be used to demonstrate that mixing along the O_2/ASW interface is limited to high temperatures and does not have a significant effect on our measurements of the crack length distribution. Bar-Nun et al.[16,17] observed numerous additional desorption peaks for a variety of gas/H_2O combinations; however, these additional peaks were not observed for the single monolayer of O_2, which is the focus of this letter. We have observed diverse desorption peaks generally consistent with the work of Bar-Nun et al. for multilayers of O_2, Ar, Kr, and CH_4 covered by ASW, although a full discussion of these various combinations is beyond the scope of this work. In summary, the first O_2 desorption peak provides information on cracks that have formed across the H_2O overlayer. The second desorption peak represents O_2 for which a path through the H_2O overlayer did not form, so that desorption of O_2 does not occur until the H_2O overlayer desorbs. Comparing the amount released by eruption of the molecular volcano versus the amount trapped beneath the H_2O allows us to quantify the length distribution of cracks formed through the H_2O overlayer during crystallization.

The fraction of O_2 trapped by H_2O is determined from the ratio of the area beneath the high-temperature desorption peak (170−190 K) to the total O_2 area. The resulting figure of merit is called the "trapped fraction". When the trapped fraction is plotted against the ASW overlayer thickness, a smoothly varying sigmoidal curve is established (Figure 2a). Below 200 ML of ASW, the O_2 trapped fraction increases slowly, implying that most crystallization-induced cracks readily span the entire thickness, opening a path for all O_2 to desorb. The trapped fraction then increases rapidly until all O_2 is trapped at thicknesses above 600 ML. The rapid increase in trapped fraction indicates that increasing numbers of cracks are unable to span the thicker ASW, increasing the amount of trapped O_2. The sigmoidal shaped data in Figure 2a was fit with eq 1, which was chosen because of its ability to consistently and accurately fit the resulting sigmoids.

$$F(L) = 1 - \Sigma A_i e^{-(L/\Lambda_i)^{n_i}} \quad (1)$$

For Figure 2a, two terms with fit parameters A_i, Λ_i, and n_i were sufficient to produce an exceptional fit relating the water overlayer thickness, L, to the trapped fraction, $F(L)$, with $R^2 > 0.999$. The quality of this fit emphasizes the continuity and quality of the obtained data, while also enabling the determination of a continuous crack length distribution.

The vertical length distribution of crystallization-induced cracks through ASW is determined by taking the derivative of the best fit (using eq 1) through the trapped fraction data (Figure 2b). Obviously, in thinner ASW films the maximum crack length is limited to the thickness of the overlayer, and as such the distribution curve represents the amount of ASW that cracks can span in very thick ASW. At low ASW coverage (<100 ML), there is an uptick in the crack length distribution curve. We believe this is due to the limited amount of O_2 that

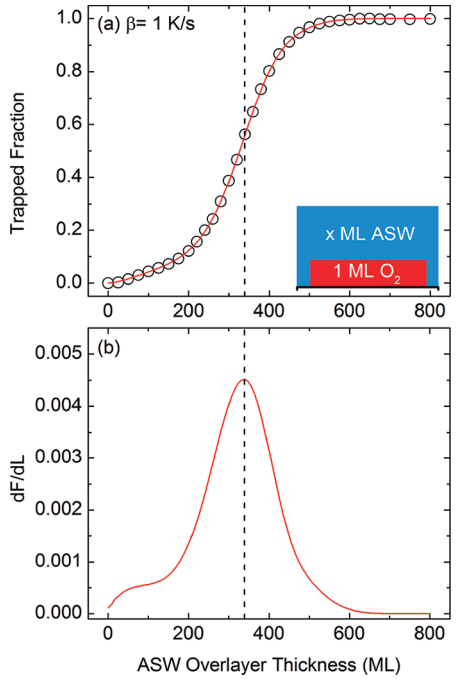

Figure 2. (a) Fraction of 1 ML O_2 trapped (○) versus increasing ASW coverage for a series of TPD heated at a ramp rate of 1 K/s. The line is a fit to the data using eq 1. (b) The derivative of the sigmoid (—) in (a) gives the distribution of vertical crack lengths formed during the crystallization of ASW.

becomes distributed within the ASW overlayer, most likely during either ASW deposition or through limited cracking around the O_2/ASW interface. O_2 inside the ASW film is isolated from the long cracks which form an escape path from the O_2 underlayer to the vacuum. Because this isolated O_2 is within the ASW overlayer, it desorbs between the volcano and trapping peaks, ultimately leading to the "bump" at ~50 ML in Figure 2b. Above ~200 ML of ASW coverage, the amount of trapping increases rapidly, with the rate peaking at 340 ML. This value corresponds to the mean crack length formed through thick ASW during crystallization. The rate of increase in the trapped fraction slows after this point, trending back toward zero as all O_2 is trapped. Increasing the coverage of ASW also increases the temperature of the volcano and trapping peaks, which, when combined with spectroscopic measurements, provides important insights into the mechanism of crack propagation.

RAIRS provides additional information about the crystallization of H_2O and the directionality of crack formation. The transition of ASW to crystalline ice is indicated by the growth of a red-shifted O−H stretching peak at ~3300 cm^{-1}. Changes in this region were monitored during TPD to relate the desorption of O_2 to the crystallization of ASW.[3,13] A sample contour plot of a time (temperature) series of infrared spectra of the O−H stretching region for 100 ML of H_2O ramped to 200 K at 1 K/s is shown in Figure 3a. These spectra indicate a dramatic increase in absorbance at 154.9 K (as shown by the dashed line), enabling unambiguous determination of the onset of crystallization. Frequency cuts taken through the RAIRS spectra for a variety of ASW overlayer thicknesses are shown in Figure 3b. Peak intensity and position are thickness dependent because of optical effects arising from the reflection geometry.[18] Due to these effects, cuts in Figure 3b are taken at the wavenumber where the difference between the initial and final

dx.doi.org/10.1021/jz201648g | J. Phys. Chem.Lett. 2012, 3, 327−331

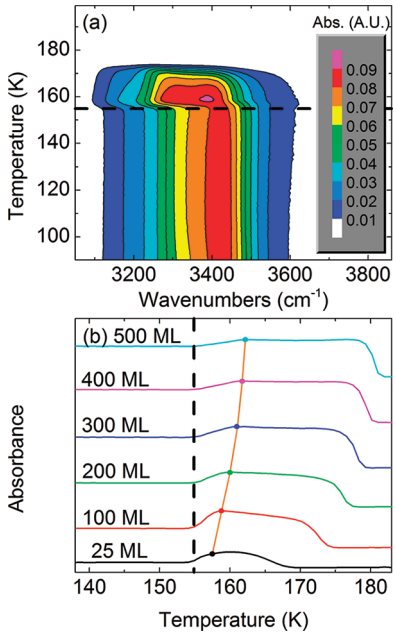

Figure 3. (a) Contour plot of the OH stretch region for 100 ML ASW ramped to 200 K at 1 K/s. (b) Frequency cuts through RAIRS spectra at different ASW overlayer thicknesses, peak of volcano eruption marked by a dot. Dashed lines indicate the onset of crystallization.

spectra is greatest, a range of 3251−3315 cm^{-1} depending on the thickness of ASW. The vertical dashed line at 154.9 K corresponds to that in Figure 3a and marks the mean position where absorbance begins to increase, an indication of the onset of crystallization. Crystallization of each sample begins at nearly the same temperature, within the ∼1 K temperature resolution of the RAIRS experiment. Thus, crystallization (and by inference cracking) initiates at approximately the same moment (temperature) irrespective of ASW thickness. These observations are consistent with previous reports indicating that ASW films in this thickness range have bulk-like crystallization kinetics.[19,20] By contrast, the O_2 "molecular volcano" peak shifts from 157 to 162 K with increasing overlayer thickness, indicating that it takes longer for cracks to span thicker ASW layers. This observation has two important implications. First, it is strong evidence that cracks propagate on the time scale of the experiment, i.e., cracks do not "instantaneously" span the ASW. This means that it should be possible to determine the kinetics of crack propagation, an effort outside the scope of this work but which is currently being pursued. Second, it proves that cracks do not initiate from random evenly dispersed nuclei, because if they did, the onset of the molecular volcano would be thickness independent. In fact, this observation was our first indication that cracks propagate from the ASW/vacuum interface. In the following section, the directionality of crack formation/propagation is conclusively demonstrated by the selective incorporation of layers of Kr and O_2 within 340 ML of ASW.

Desorption of O_2 and Kr from different positions in 340 ML of ASW conclusively illustrates the direction of crack formation during the crystallization of ASW (Figure 4). In this series, 1 ML of O_2 is fixed at the bottom of 340 ML of ASW, while 1 ML of Kr is placed at different quartiles within the same 340 ML ASW film. The Kr location ranges from being directly on top of O_2 and underneath 340 ML ASW (Figure 4a) to being underneath 85 ML of ASW and separated from O_2 by 255 ML

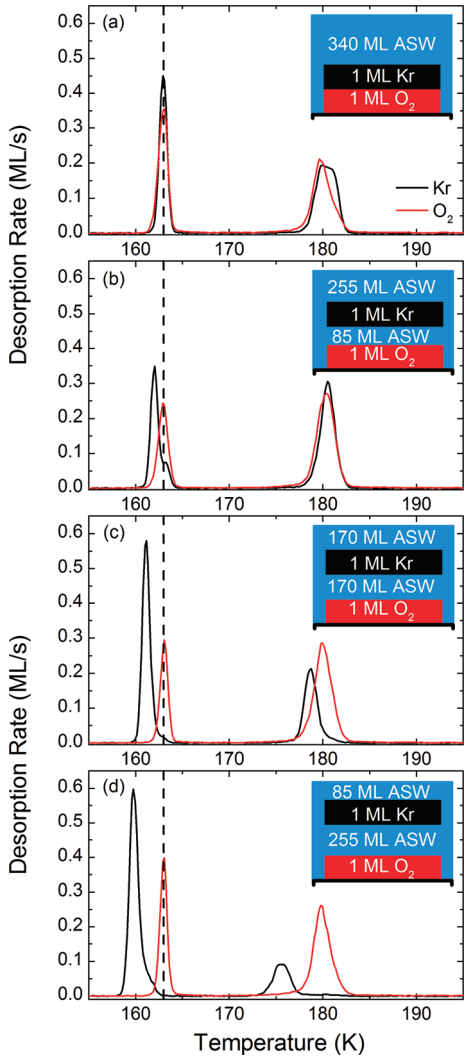

Figure 4. Series of TPD spectra for 1 ML O_2 covered by 340 ML of ASW and 1 ML of Kr placed at various locations in the overlayer. In (a) the Kr and O_2 are below 340 ML of ASW, while the layers are separated by 85 ML ASW in (b), 170 ML in (c), and 255 ML in (d).

ASW (Figure 4d). Examining the TPD spectra in Figure 4, notice that the position of the two O_2 desorption peaks remains constant in all four experiments (Figure 4a−d), while the Kr peaks shift to lower temperature as the amount of ASW above Kr decreases. The decrease in the temperature of the Kr volcano peak is consistent with cracks forming at the outer surface of ASW and traveling down to release the Kr volcano and then traveling further to release the O_2 volcano at a higher temperature. If cracks originated in the middle or at the bottom of the H_2O layer, the O_2 and Kr would desorb at the same temperature. Similarly, the Kr trapping peak position is a function of the amount of ASW above the Kr layer. Kr placed closer to the top surface of the ASW is exposed at lower temperatures because the thinner trapping overlayer "runs out" of H_2O at a lower temperature. Interestingly, when the Kr and O_2 layers are close to one another, as in Figure 4b, the Kr and O_2 volcano peaks are well resolved while the Kr and O_2 trapping peaks remain atop one another. This implies that mixing at the O_2/ASW interface does not occur until after the molecular volcano and thus does not impact the crack length distribution. The behavior observed in Figure 4 is independent

dx.doi.org/10.1021/jz201648g | J. Phys. Chem.Lett. 2012, 3, 327−331

of composition, and similar behavior is observed with O_2 on top and Kr on the bottom as well as with O_2/O_2 and O_2/Ar (data not shown).

We have defined two distinct desorption regimes of O_2 covered by ASW, one corresponding to crystallization-induced cracking known as the "molecular volcano", and a second higher temperature peak that corresponds to O_2 trapped beneath the H_2O layer after crystallization. Monitoring the degree of trapping as a function of ASW overlayer thickness allowed us to determine the vertical length distribution of cracks formed through ASW during crystallization. Additionally, utilizing a combination of RAIRS and TPD measurements, cracks were shown to originate at the ASW/vacuum interface. Understanding the mechanism for the release of trapped gases from ASW is crucial to modeling outgasing from various ices of current astrophysical interest.[4−7] Future work will focus on determining how the crack length distribution depends on factors such as the heating rate, underlayer composition, and underlayer thickness.

EXPERIMENTAL SECTION

Experiments were performed on a 1-cm diameter Pt(111) substrate cooled to a base temperature of ~20 K in an ultrahigh vacuum system (UHV), described previously,[3,21] with a base pressure of $<1 \times 10^{-10}$ Torr. Temperature is controlled up to 1200 K by resistive heating and measured by a type K thermocouple spot-welded to the back of the substrate and calibrated to an accuracy of better than ±2 K by controlled desorption of Kr and H_2O. Graphene was deposited by heating the Pt(111) substrate to 1100 K in the presence of decane, and the layer integrity was verified by the desorption of Kr and H_2O. The species O_2 (Nor Lab UHP) and H_2O (doubly distilled 18 MΩ-cm) were deposited at normal incidence via quasi-effusive molecular beams. The O_2 beam passed through four differential pumping stages before impinging on the sample at a rate of 0.28 ML/s with a diameter of 0.75 cm. The H_2O beam was collimated by three differential pumping stages before impinging on the sample at a rate of 0.87 ML/s with a beam diameter slightly larger than the 1 cm Pt(111) substrate. TPD spectra were collected at a ramp rate of 1 K/s utilizing an Extrel quadrapole mass spectrometer monitoring at m/z = 18 for H_2O and m/z = 32 for O_2, and the linearity of the detector response was verified across 2 orders of magnitude by the controlled deposition of O_2 on graphene. Infrared spectra were acquired with a Bruker Equinox 55 at an 82° ± 1° angle of incidence utilizing a mercury cadmium telluride (MCT) detector.

AUTHOR INFORMATION

Corresponding Authors

*E-mail: Scott.Smith@pnnl.gov (R.S.S.).
*E-mail: Bruce.Kay@pnnl.gov (B.D.K.).

Notes

The authors declare no competing financial interest.

ACKNOWLEDGMENTS

This work was supported by the U.S. Department of Energy (DOE), Office of Basic Energy Sciences, Division of Chemical Sciences, Geosciences, and Biosciences. Pacific Northwest National Laboratory (PNNL) is a multiprogram national laboratory operated for DOE by Battelle. The research was performed using EMSL, a national scientific user facility sponsored by DOE's Office of Biological and Environmental Research and located at Pacific Northwest National Laboratory.

REFERENCES

(1) Smith, R. S.; Petrik, N. G.; Kimmel, G. A.; Kay, B. D. Thermal and Nonthermal Physiochemical Processes in Nanoscale Films of Amorphous Solid Water. *Acc. Chem. Res.* **2011**, DOI: 10.1021/ar200070w.

(2) Smith, R. S.; Zubkov, T.; Dohnalek, Z.; Kay, B. D. The Effect of the Incident Collision Energy on the Porosity of Vapor-Deposited Amorphous Solid Water Films. *J. Phys. Chem. B* **2009**, *113*, 4000−4007.

(3) Smith, R. S.; Zubkov, T.; Kay, B. D. The Effect of the Incident Collision Energy on the Phase and Crystallization Kinetics of Vapor Deposited Water Films. *J. Chem. Phys.* **2006**, *124*, 114710−114717.

(4) Mautner, M. N.; Abdelsayed, V.; El-Shall, M. S.; Thrower, J. D.; Green, S. D.; Collings, M. P.; McCoustra, M. R. S. Meteorite Nanoparticles as Models for Interstellar Grains: Synthesis and Preliminary Characterisation. *Faraday Discuss.* **2006**, *133*, 103−112.

(5) Collings, M. P.; Anderson, M. A.; Chen, R.; Dever, J. W.; Viti, S.; Williams, D. A.; McCoustra, M. R. S. A Laboratory Survey of the Thermal Desorption of Astrophysically Relevant Molecules. *Mon. Not. R. Astron. Soc.* **2004**, *354*, 1133−1140.

(6) Hogerheijde, M. R.; Bergin, E. A.; Brinch, C.; Cleeves, L. I.; Fogel, J. K. J.; Blake, G. A.; Dominik, C.; Lis, D. C.; Melnick, G.; Neufeld, D.; et al. Detection of the Water Reservoir in a Forming Planetary System. *Science* **2011**, *334*, 338−340.

(7) Goldsmith, P. F.; Liseau, R.; Bell, T. A.; Black, J. H.; Chen, J.-H.; Hollenbach, D.; Kaufman, M. J.; Li, D.; Lis, D. C.; Melnick, G.et al.Herschel Measurements of Molecular Oxygen in Orion. *Arxiv* 2011, 1108.0441v1.

(8) Ayotte, P.; Smith, R. S.; Stevenson, K. P.; Dohnalek, Z.; Kimmel, G. A.; Kay, B. D. Effect of Porosity on the Adsorption, Desorption, Trapping, and Release of Volatile Gases by Amorphous Solid Water. *J. Geophys. Res., [Planets]* **2001**, *106*, 33387−33392.

(9) May, R. A.; Smith, R. S.; Kay, B. D. Probing the Interaction of Amorphous Solid Water on a Hydrophobic Surface: Dewetting and Crystallization Kinetics of ASW on Carbon Tetrachloride. *Phys. Chem. Chem. Phys.* **2011**, *13*, 19848−19855.

(10) Smith, R. S.; Huang, C.; Wong, E. K. L.; Kay, B. D. The Molecular Volcano: Abrupt CCl_4 Desorption Driven by the Crystallization of Amorphous Solid Water. *Phys. Rev. Lett.* **1997**, *79*, 909−912.

(11) May, R. A.; Kondrachova, L.; Hahn, B. P.; Stevenson, K. J. Optical Constants of Electrodeposited Mixed Molybdenum-Tungsten Oxide Films Determined by Variable-Angle Spectroscopic Ellipsometry. *J. Phys. Chem. C* **2007**, *111*, 18251−18257.

(12) Kimmel, G. A.; Petrik, N. G.; Dohnalek, Z.; Kay, B. D. Crystalline Ice Growth on Pt(111): Observation of a Hydrophobic Water Monolayer. *Phys. Rev. Lett.* **2005**, *95*, 166102.

(13) Smith, R. S.; Matthiesen, J.; Knox, J.; Kay, B. D. Crystallization Kinetics and Excess Free Energy of H_2O and D_2O Nanoscale Films of Amorphous Solid Water. *J. Phys. Chem. A* **2011**, *115*, 5908−5917.

(14) McClure, S. M.; Barlow, E. T.; Akin, M. C.; Safarik, D. J.; Truskett, T. M.; Mullins, C. B. Transport in Amorphous Solid Water Films: Implications for Self-Diffusivity. *J. Phys. Chem. B* **2006**, *110*, 17987−17997.

(15) McClure, S. M.; Safarik, D. J.; Truskett, T. M.; Mullins, C. B. Evidence that Amorphous Water below 160 K Is Not a Fragile Liquid. *J. Phys. Chem. B* **2006**, *110*, 11033−11036.

(16) Laufer, D.; Kochavi, E.; Barnun, A. Structure and Dynamics of Amorphous Water Ice. *Phys. Rev. B* **1987**, *36*, 9219−9227.

(17) Barnun, A.; Kleinfeld, I.; Kochavi, E. Trapping of Gas-Mixtures by Amorphous Water Ice. *Phys. Rev. B* **1988**, *38*, 7749−7754.

(18) Cholette, F.; Zubkov, T.; Smith, R. S.; Dohnalek, Z.; Kay, B. D.; Ayotte, P. Infrared Spectroscopy and Optical Constants of Porous Amorphous Solid Water. *J. Phys. Chem. B* **2009**, *113*, 4131−4140.

(19) Lofgren, P.; Ahlstrom, P.; Lausma, J.; Kasemo, B.; Chakarov, D. Crystallization Kinetics of Thin Amorphous Water Films on Surfaces. *Langmuir* **2003**, *19*, 265−274.
(20) Smith, R. S.; Kay, B. D. Molecular Beam Studies of Kinetic Processes in Nanoscale Water Films. *Surf. Rev. Lett.* **1997**, *4*, 781−797.
(21) Zubkov, T.; Smith, R. S.; Engstrom, T. R.; Kay, B. D. Adsorption, Desorption, and Diffusion of Nitrogen in a Model Nanoporous Material. I. Surface Limited Desorption Kinetics in Amorphous Solid Water. *J. Chem. Phys.* **2007**, *127*, 184707.